catalysts

MDPI

Article

Intercalated-Laurate-Enhanced Photocatalytic Activities of Ni/Cr-Layered Double Hydroxides

Xuehua Zhang [1,2], Zili Jiang [1,2], Fengting Sun [1,2], Yuhan Chen [3], Changrong Shi [4,5], Zhanying Zhang [4,5], Guangren Qian [1,2] and Xiuxiu Ruan [1,2,*]

[1] School of Environmental and Chemical Engineering, Shanghai University, No. 99 Shangda Road, Shanghai 200444, China
[2] Center of Green Urban Mining & Industry Ecology, Shanghai University, No. 99 Shangda Road, Shanghai 200444, China
[3] School of Mechanical and Automotive Engineering, Shanghai University of Engineering Science, No. 333 Longteng Road, Shanghai 261600, China
[4] School of Mechanical, Medical and Process Engineering, Faculty of Engineering, Queensland University of Technology, Brisbane, QLD 4000, Australia
[5] Centre for Agriculture and the Bioeconomy, Queensland University of Technology, Brisbane, QLD 4000, Australia
* Correspondence: ruanxiuxiu@shu.edu.cn; Tel.: +86-021-66137742

Abstract: Laurate (LA^-)-intercalated nickel–chromium-layered double hydroxides (LDHs) were synthesized using the co-precipitation method and investigated as a potential photocatalyst for methylene orange (MO) degradation. For comparison, a series of LDHs with various molar ratios of Ni^{2+}(or Mg^{2+})/Cr^{3+}(or Fe^{3+})/LA^-(or $CO3^{2-}$) were prepared. X−ray diffraction (XRD) and element analysis showed that Ni/Cr(2/1)−1.0 LA LDH had the most ordered crystal structure, and showed the same photocatalytic decolorization performance as Mg/Cr(2/1)−1.0LA LDH towards MO, which was significantly superior to Ni/Cr−CO_3 LDH, Ni/Fe(2/1)−1.0LA LDH, and Ni/Cr−CO_3 LDH with LA^-, and Cr^{3+} with LA^-. The photocatalytic removal rate of MO with the initial concentration of 100 mg/L by Ni/Cr(2/1)−1.0LA LDH (0.5 g/L) could be up to 80% with UV light irradiation for 3 h, which was almost twice higher than that of the sorption test. The photocatalytic reaction was in accordance with the pseudo-first-order kinetics, which implied that the catalytic process took place on the surface of the catalyst. All the results indicate the photodegradation of MO by Ni/Cr−LA LDHs was enhanced by the sorption of MO onto the intercalated LA^- in the interlayer. The free radical capture experiments suggest that the main role of the photocatalytic mechanism of Ni/Cr−LA LDHs could be the $\bullet O_2^-$ with high oxidation activity produced by the electron-hole pairs of LDH, as excited by UV light. Additionally, the $\bullet O_2^-$ further reacted with the adjacent MO molecule pre-sorbed on the intercalated LA.

Keywords: organic Ni/Cr LDH; photocatalysis; methyl orange

check for updates

Citation: Zhang, X.; Jiang, Z.; Sun, F.; Chen, Y.; Shi, C.; Zhang, Z.; Qian, G.; Ruan, X. Intercalated-Laurate-Enhanced Photocatalytic Activities of Ni/Cr-Layered Double Hydroxides. *Catalysts* **2023**, *13*, 698. https://doi.org/10.3390/catal13040698

Academic Editor: Lucjan Chmielarz

Received: 3 March 2023
Revised: 29 March 2023
Accepted: 31 March 2023
Published: 4 April 2023

Copyright: © 2023 by the authors. Licensee MDPI, Basel, Switzerland. This article is an open access article distributed under the terms and conditions of the Creative Commons Attribution (CC BY) license (https://creativecommons.org/licenses/by/4.0/).

1. Introduction

Layered double hydroxides (LDHs) are lamellar compounds that consist of interlayer exchangeable anions and positively charged laminates; hydrotalcite and hydrotalcite-like compounds are examples of LDHs that have been widely studied. The general representative formula of LDHs is $[M^{2+}_{1-x}M^{3+}_{x}(OH)_2]$ $(A^{n-})_{x/n-}\cdot yH_2O$, where A^{n-} is the interlayer exchangeable negatively charged anion; M^{2+} and M^{3+} are divalent and trivalent metal cations, respectively; and x is the molar ratio of $M^{3+}/(M^{2+} + M^{3+})$, which varies from 0.22 to 0.33 [1–5]. LDHs are an important layered material, which has been highly valued in important fields such as adsorption [6], electrochemistry [7], biomedical science [8], catalysis [9], photocatalysis [10,11], photochemistry [12], and environmental applications.

Recently, LDHs have proven to be a ground-breaking photocatalyst group in the fields of energy and environment, which is attributed to their several excellent properties. The

unique layered structure, uniform distribution of several metal cations in the laminate, surface hydroxyl groups, flexible adjustability, intercalated exchangeable anions with interlayer spaces, swelling properties, oxo-bridged linkage, and high chemical stability are some of the important advantages of LDHs in photocatalytic applications [13–15]. Normally, the study of LDH in photocatalysis has focused on inorganic LDH. Mg/Al hydrotalcites were first reported as the photocatalyst for the degradation of 4-chlorophenol and p-cresol [16], in which Mg/Al hydrotalcites were known to perform as an induced semiconductor and termed as a photo-assisted system instead of photocatalysts because of their high photocatalytic activity. In this case, the photoexcitation induced in the laminar structure of LDH may lead to charge migration and the formation of photoactive defects [16], which may improve photocatalytic performance. Ni/Ti-LDHs displayed great performance in the photocatalytic degradation of methylene blue dye due to their high specific surface area, porous structure, lower band gap, and different surface states of nickel and titanium in the laminate and in the presence of defects [17]. Similarly, $Ni(OH)_2$-CdS/RGO composites showed high photocatalytic hydrogen production activity, and the result indicated sodium hydroxide was an excellent co-catalyst to enhance photocatalytic activity [18]. Some studies have reported the application of the chromium-based transitional metal octahedron of inorganic materials in photocatalysis. Since the LDH was based on brucite-like layers with edge-shared $M(OH)_6$ octahedra, Cr^{3+} ions in the CrO_6 octahedron of Zn/Cr−CO_3 LDHs played an important role in photocatalysis [19]. Cu/Ni/Zn/Cr LDHs showed a significant photodegradation ability toward Rhodamine B, Congo red, chlorinated phenol, and salicylic acid under visible-light irradiation [19]. In addition, Ni-doped ZnCr-LDHs showed more excellent photocatalytic performance than traditional LDHs [20]. In the oxygen evolution reactions (OER) of 14 kinds of $M^{2+}{}_n/M^{3+}$ LDHs (M^{2+} = Mg, Co, Ni, Cu, and Zn; M^{3+} = Cr and Fe; n = 2, 3, and 4), Ni_n/Cr LDHs (n = 2, 3, and 4) were efficient OER photocatalysts, among which Ni_2/Cr LDH showed the most active photocatalytic OER performance [21]. Research has demonstrated that transition metals, such as Ni and Cr, are outstanding candidates for LDH photocatalysts.

As stated above, the photocatalytic activity of inorganic LDH often depended on the crystallite structure and the specific area. A large specific area will facilitate the contact of the contaminant and catalyst, while a small internal surface and interlamellar spacing hinder the separation of electrons and holes [22]. Therefore, expanding the interlayer gallery could be critical for the application of LDHs as good photocatalysts. Surfactant intercalation into the interlayer of LDH has been used to improve the sorption efficiencies of organic contaminants, which is mainly due to the hydrophobic organic phase in the interlayer [23,24]. For example, the DS- and sebacate anion intercalated into the Mg/Al LDH interlayer can greatly enhance the adsorption capacity of alachlor and metolachlor from water [25]. Moreover, intercalating specific surfactant intercalation may also have a positive effect on enhancing the photocatalytic activity of the material. For instance, organic UV−absorbent-intercalated Zn/Al LDHs showed outstanding UV photostability in polypropylene composites [26]. Increasing the concentration of intercalated SDS into the Zn/Cd/Al LDH significantly improved the photocatalytic activity [27]. However, the relationships between the photocatalytic activity and sorption capacities of organic-phase-intercalated LDH are not clear, and their photocatalytic mechanism needs to be further explored.

In this study, a series of laurate (LA^-)-intercalated nickel–chromium-layered double hydroxides (LDHs) (Ni/Cr−LA LDH) were prepared using the co-precipitation method and characterized by using X−ray diffraction (XRD), diffuse reflectance UV−vis spectra, photoluminescence spectroscopies, Fourier-transform infrared spectroscopy (FT−IR), and elemental analysis (EA). Methyl orange (MO) was chosen as a typical contaminant to evaluate the photocatalytic performance of the as-prepared LDHs with UV light. A possible mechanism of the intercalated-laurate-enhanced photocatalytic activities of Ni/Cr LDHs was analyzed and discussed by using a kinetic model and quenching experiment. The

information from this study will benefit the design of unique photocatalysis materials based on LDHs.

2. Results and Discussion

2.1. Physicochemical Characterization of the Catalysts

2.1.1. Elemental Analysis of LDHs

The elemental compositions of Ni/Cr LDHs are listed in Table 1. With the increase in the expected molar ratio of Ni/Cr, the content of Ni in LDH increased continuously, and the content of Cr decreased. The actual molar ratios of Ni to Cr were calculated and found to be very close to the expected molar ratio value for all samples. The carbon content of Ni/Cr−LA LDHs reduced with the decrease in the theoretical dosage of laurate. With the increase in the molar ratio of Ni/Cr, the carbon content of Ni/Cr−LA LDHs gradually decreased. Additionally, when the molar ratio of Ni/Cr increased from 2 to 3, the carbon content was reduced, obviously due to the decreased charge density of LDHs.

Table 1. Elemental analysis of Ni/Cr−LA LDHs.

Samples	C (%)	N (%)	Ni^{2+} (mg/g)	Cr^{3+} (mg/g)	Ni^{2+}/Cr^{3+} (mol/mol)	Band Gap (eV)
Ni/Cr(2/1)-1.0LA LDH	26.7	0.270	230.7	112.7	1.81	4.31
Ni/Cr(2/1)-0.5LA LDH	14.6	0.980	218.5	104.1	1.85	4.10
Ni/Cr(1/1)-1.0LA LDH	27.7	0.315	162.3	155.7	0.92	/
Ni/Cr(3/1)-1.0LA LDH	21.4	0.754	273.9	92.3	2.63	/

2.1.2. X−ray Diffraction (XRD) Analysis

The XRD patterns of Ni/Cr−LA LDHs are shown in Figure 1a,b. The XRD pattern for organic LDHs suggests a d_{003} of 2.80 nm for Ni/Cr(2/1)−1.0LA LDH, which is much higher than that of inorganic LDH (0.77 nm), as shown in Figure S1. These results indicate that the interlayer spacing of Ni/Cr LDH was increased due to the intercalation of laurate, which is similar to previous studies [28,29]. Ni/Cr(2/1)−1.0LA LDH showed an obvious signal at the characteristic peaks ((003) and (006)) of layered double hydroxide phases in the X−ray diffraction patterns [28,29], while the diffraction peak became weaker with the decreased dosage, as shown in Figure 1a. These results demonstrate that the crystal structures of Ni/Cr LA LDHs were more ordered when the laurate content increased. Figure 1b shows that the characteristic peak (d_{003}) of Ni/Cr(2/1)−1.0LA LDH was the sharpest, and the half-peak width was also small, indicating that Ni/Cr(2/1)−1.0LA LDH has a good crystal shape. When Ni/Cr = 3, the half-peak width of LDH increases significantly, indicating the high Ni content was not conducive to the formation of organic LDH crystal.

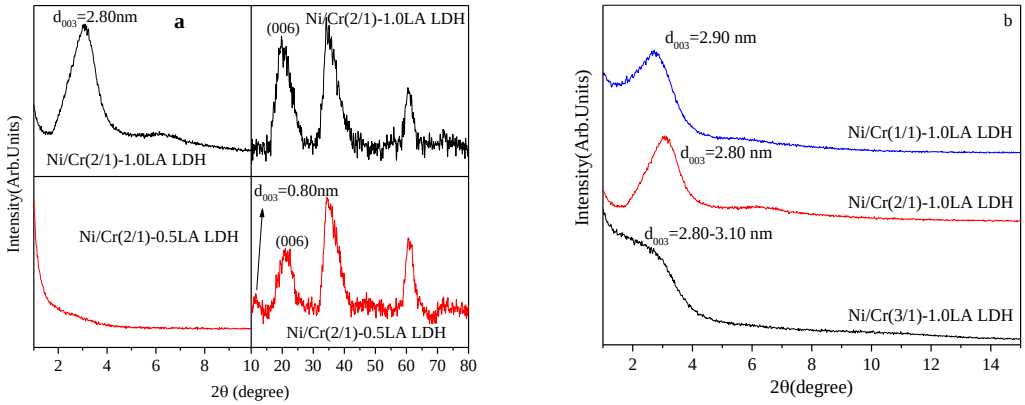


Figure 1. *Cont.*

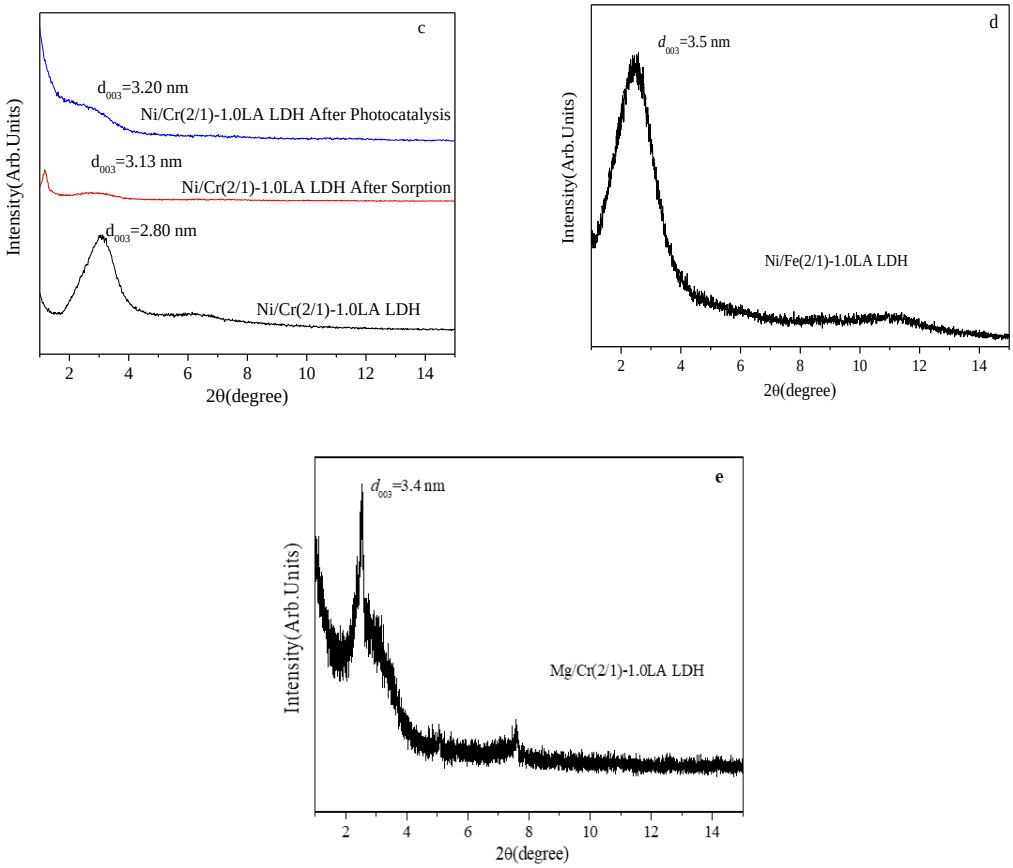


Figure 1. The XRD patterns of (**a**) Ni/Cr(2/1)−xLA LDH (x = 1.0, 0.5) at narrow-angle and wide-angle, (**b**) Ni/Cr−1.0LA LDH (Ni/Cr = 1, 2, 3), (**c**) Ni/Cr (2/1)−1.0LA LDH after adsorption and catalysis, (**d**) Ni/Fe(2/1)−1.0LA LDH, and (**e**) Mg/Cr(2/1)−1.0LA LDH.

The XRD patterns of Ni/Cr(2/1)−1.0LA LDHs after photocatalysis and sorption are shown in Figure 1c. The d_{003} values of Ni/Cr(2/1)−1.0LA LDHs after photocatalysis and sorption were significantly higher than that of the original LDH, suggesting that MO would enter the Ni/Cr(2/1)−1.0LA LDH interlayer after the reaction.

The XRD patterns of Ni/Fe(2/1)−1.0LA LDHs and Mg/Cr(2/1)−1.0LA LDHs are shown in Figure 1d,e, respectively. The characteristic peaks (003) of organic LDH appeared in the XRD patterns of Ni/Fe(2/1)−1.0LA LDH and Mg/Cr(2/1)−1.0LA LDH [28,29], indicating that the organic LDH structures were formed successfully.

2.1.3. Scanning Electron Microscope (SEM)

The SEM images of (a) Ni/Cr(2/1)−1.0LA LDH and (b) Ni/Cr(2/1) LDH are shown in Figure S2. Figure S2a indicates the apparent particle agglomeration of Ni/Cr(2/1)−1.0LA LDH with the organic anion intercalation, while the microscopic hexagonal lamellar structure of LDH is not obvious. Additionally, the surface of Ni/Cr(2/1)−1.0LA LDH was rough. In contrast, the particles of inorganic LDH were more dispersed, the typical pseudo-hexagonal structure, as reported, could be clearly observed in the red area [5], and the surface was relatively smooth (Figure S2b).

2.1.4. Fourier-Transform Infrared Spectroscopy Analysis (FT−IR)

The typical features of LDHs and the presence of laurate in the Ni/Cr LDH could be further evidenced by the FT−IR spectra (Figure 2). The FT−IR spectra of all samples demonstrate the characteristics of the hydrotalcite phase, as shown in Figure 2. The presence of laurate in the Ni/Cr-LA LDHs was confirmed by the characteristic band of the CH_3 stretching vibrations at 2956–2852 cm^{-1} and vibration bands at 1556 and 1410 cm^{-1}, which

correspond to antisymmetric and symmetric stretching vibrations of the COO^- [28,30,31]. The band for COO^- of the Ni/Cr(2/1)−xLA LDH(x = 0.5, 1) showed a red shift compared with the pure laurate. The red-shift phenomenon was more obvious with the lower laurate dosage. Furthermore, the intensity of the vibrational peaks of the functional groups gradually decreased with the decrease in laurate dosage, which is in agreement with the XRD results.

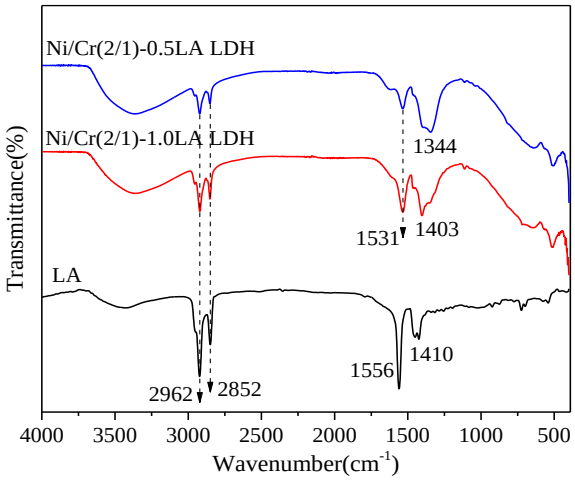


Figure 2. FT−IR spectroscopy of LA and Ni/Cr(2/1)−xLA LDH (x = 1.0, 0.5).

2.2. Photochemical Properties

Figure 3 shows the diffuse reflectance UV−vis−NIR spectra of the catalysts. All the Ni/Cr LDHs showed an absorption band in the range of 200–300 nm, as shown in the UV−vis−NIR diffuse reflectance patterns, owing to ligand-to-metal charge transfer (LMCT) from the 2p orbital of oxygen to the 3d orbital of M^{2+} (O 2p → Ni 3d t2g) and Cr^{3+} ions (O 2p → Cr 3d t2g) in the MO_6 octahedra of the LDHs [32]. Nakamura et al. reported the visible-light-induced metal-to-metal charge transfer (MMCT) due to oxo-bridge bimetallic linkages, which allowed photoactive regions to extend into the visible range [33]. Therefore, the strong absorption band between 500 and 800 nm in the visible region can be attributed to Ni^{2+} and Cr^{3+} ions and the formation of the MMCT of Ni^{II}−O−Cr^{III} oxo-bridge bimetallic linkages in the LDH brucite layers [34]. The absorption intensity was negatively correlated with laurate content, which means less laurate would be beneficial to improve the light absorption capacity of the LDH.

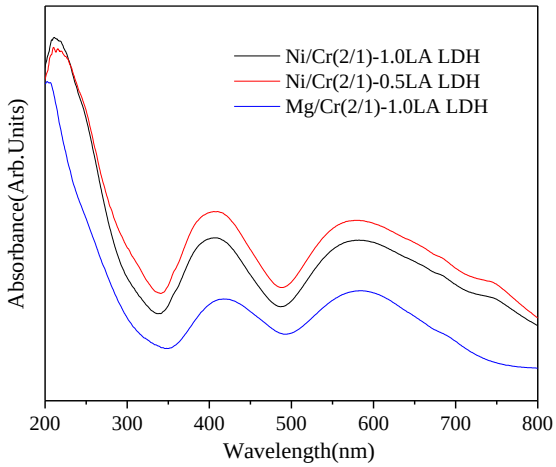


Figure 3. Diffuse reflectance UV−vis spectra of Ni/Cr(2/1)−xLA LDH(x = 1.0, 0.5) and Mg/Cr(2/1)−1.0LA LDH.

The band gaps of Ni/Cr(2/1)−xLA LDHs are determined by Equation (1) [35]:

$$(h\alpha\nu)^{1/n} = A(h\nu - E_g) \quad (1)$$

where h, α, ν, and A are the Planck constant, absorption coefficient, light frequency, and proportionality constant, respectively; n determines the transition characteristics in semiconductors, that is, the indirect transition (n = 4) or direct transition (n = 1). In this study, since the absorbance (Abs) of the sample is proportional to α, α is replaced by Abs, and the value of n was found to be 1. Based on the relation graph of Abs$h\nu$ to $h\nu$, the values of the band gaps for the LDH photocatalysts were determined by the extrapolation method and are presented in Table 1. The band gaps of Ni/Cr(2/1)−xLA LDHs(x = 0.5, 1) were decreased by reducing the concentration of the intercalated laurate. However, the low band gap does not necessarily indicate an enhancement in the catalytic performance.

To analyze the migration and recombination of photogenerated electrons and holes in Ni/Cr−LA LDHs, the photoluminescence spectroscopies of Ni/Cr−LA LDHs are shown in Figure 4. As shown in Figure 4, the emission peaks (λ_{em}) of Ni/Cr−0.5LA LDH and Ni/Cr−1.0La LDH were around 475 nm, and the peak intensity of Ni/Cr−0.5LA LDH was weaker than that of Ni/Cr−1.0LA LDH within the emission peak range. This result indicates that Ni/Cr−0.5LA LDH can more effectively inhibit the recombination of photogenerated electrons and holes than Ni/Cr−1.0LA LDH, and then promote the transfer and separation of photogenerated carriers.

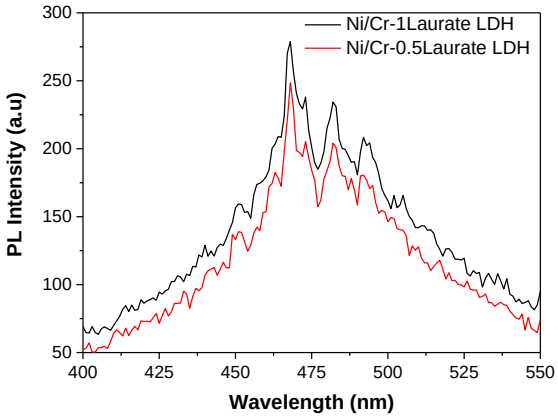


Figure 4. Photoluminescence emission spectra of Ni/Cr−xLa LDH (x = 1.0, 0.5).

2.3. Photocatalytic Performance of Ni/Cr LDHs in MO Degradation

2.3.1. Necessity of Organic-Intercalated Structure

Ni/Cr(2/1)−1.0LA LDH, Ni/Cr(2/1)−CO_3 LDH, and Ni/Cr(2/1)−CO_3 LDH mixed with the laurate solution and Cr^{3+} mixed with the laurate solution were chosen as photocatalysts in the MO photocatalytic decolorization tests to identify the high-efficiency catalyst structure. The results indicate that Ni/Cr(2/1)−1.0LA LDH showed outstanding adsorption properties and exhibited a higher photoactivity than the other samples in Figure 5. This suggests that the organic intercalated into the interlayer of the LDH structure was necessary in photocatalysis.

2.3.2. Effect of the Content of Organic Intercalated into the Interlayer

The effect of the organics intercalated into the interlayer on the photocatalytic degradation of basic dyes (MO) was studied by varying the organics' concentration (0.5 and 1.0 mol/L); the results are shown in Figure 6. The results demonstrate that Ni/Cr(2/1)−0.5LA LDH has the highest degradation efficiency for MO, and the removal rate of MO can reach 80% with UV light irradiation for 3 h. Mersly et al. [36] showed that the removal rate of acid orange 7 was only 66% over Zn/Cr−SO4 LDH with UV light irradiation within 2 h. It is well known that the photocatalytic degradation of dye is a complicated process in which

the adsorption of the dyes on the catalyst surface is the first step. The superior partition of the Ni/Cr(2/1)−xLA LDHs facilitated the dye adsorption, which would be beneficial to promote the catalytic degradation progress. The Ni/Cr(2/1)−xLA LDH samples showed almost the same adsorption capacity at the end of photocatalysis after 3 h, so the different photocatalytic performances of the different samples might be related to the photochemical characteristics. The higher photocatalysis ability of Ni/Cr(2/1)−0.5LA LDH is possibly attributed to the relatively higher utilization efficiency of UV than that of Ni/Cr(2/1)−1.0LA LDH (Figure 4).

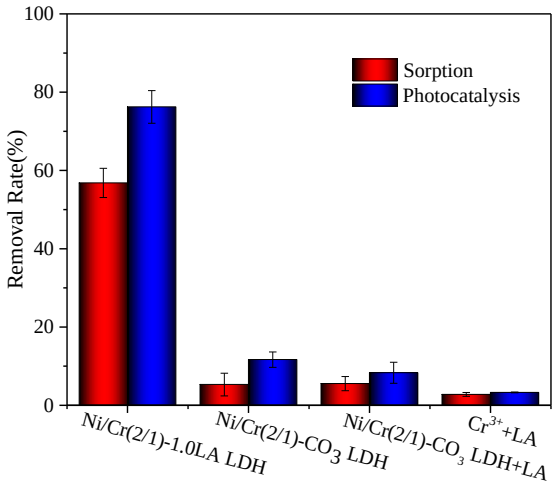


Figure 5. Photocatalytic degradation of MO over Ni/Cr(2/1)−1.0LA LDH, Ni/Cr(2/1)−CO_3 LDH, Ni/Cr(2/1)−CO_3 LDH+LA^- and Cr^{3+}+LA^-.

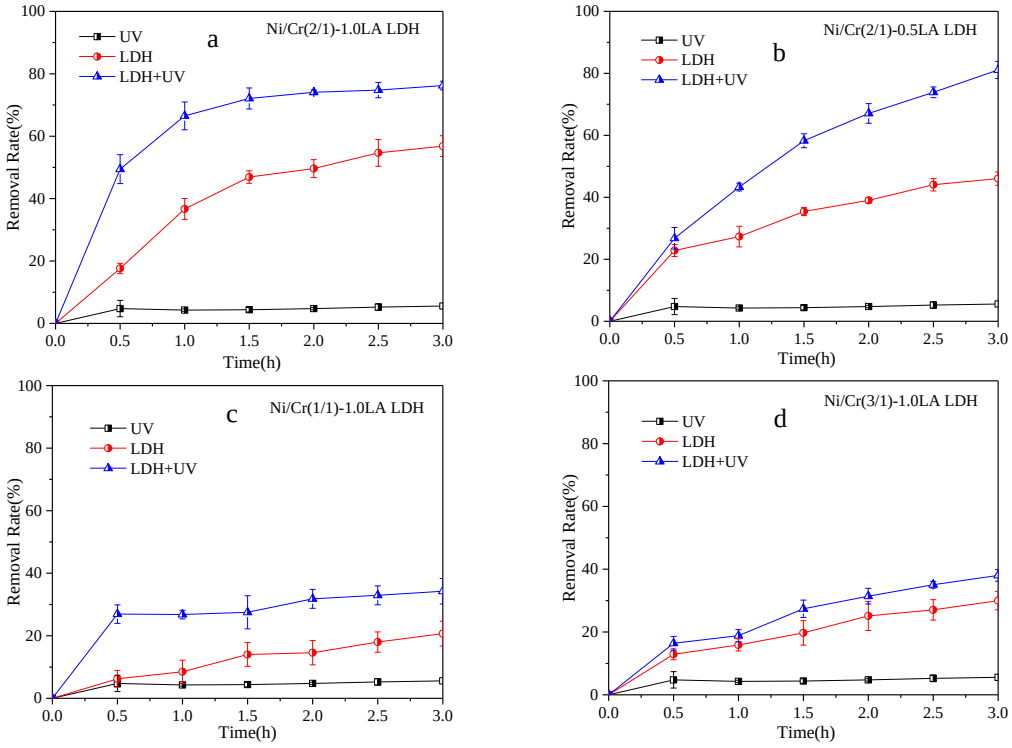


Figure 6. Photocatalytic degradation of MO over (**a**) Ni/Cr(2/1)−1.0LA LDH, (**b**) Ni/Cr(2/1)−0.5LA LDH, (**c**) Ni/Cr(1:1)−LA LDH, and (**d**) Ni/Cr(3:1)−LA LDH.

2.3.3. Positive Role of Ni and Active Effect of Cr

In this part, the influence of the Ni^{2+} ion on the photocatalytic activity of Ni/Cr−1.0LA LDH (Ni/Cr = 1, 2, and 3) for MO degradation under Hg light irradiation is addressed, and the results are presented in Figure 6. Ni/Cr(2:1)−1.0LA LDH was the most active material in the MO degradation study at 3 h. The fact that Ni/Cr(2:1)−1.0LA LDH had the highest photocatalytic activity may be attributed to the relatively regular particle shape compared with the other two samples. On the other hand, Ni/Cr(2:1)−1.0LA LDH had good sorption ability, which might be beneficial to the photocatalytic activity.

Based on the XRD patterns of the samples shown in Figure 1b, the number of stacked layers (n) of different types of LDHs was calculated by Scherrer's formula, as given in Table S1. It is obvious that the change in the metal ion ratio has an impact on the interlayer spacing of Ni/Cr−LA LDH. With the increase in Ni/Cr, the D value of LDH decreases, indicating that Ni can play a role in reducing the crystal size in Ni/Cr−LA LDH. Moreover, the stacking numbers of the three samples did not show much difference, indicating that the change in the Ni/Cr ratio does not affect the stacking of LDH sheets.

To explore the reactive metal in organic-intercalated Ni/Cr LDH, Ni^{2+} and Cr^{3+} were replaced by Mg^{2+} and Fe^{3+}, respectively (Figure 7). Compared with that shown in Figure 6a, Mg/Cr(2/1)−1.0LA LDH showed almost the same photocatalytic performance as Ni/Cr(2/1)−1.0LA LDH, while Ni/Fe(2/1)−1.0LA LDH did not show any photocatalytic activity under the same experimental conditions. The results indicate that Cr^{3+} was the reactive metal in Ni/Cr(2/1)−1.0LA LDH. In order to investigate the influence of the type and content of metal ions in LDH on photocatalytic activity, the XRD patterns of Ni/Cr(2/1)−1.0LA LDH (Figure 1a), Ni/Fe(2/1)−1.0LA LDH (Figure 1d), and Mg/Cr(2/1)−1.0LA LDH (Figure 1e) and the contents of each element in the above three samples are given in Table 2. The actual metal molar ratio of the samples was similar to the theoretical doping ratio 2. The particle size of Ni/Cr(2/1)−1.0LA LDH was the smallest. Moreover, Ni/Cr(2/1)−1.0LA LDH showed better catalytic performance than Mg/Cr(2/1)−1.0LA LDH with less Cr^{3+} content, which might be attributed to the effect of Ni^{2+}.

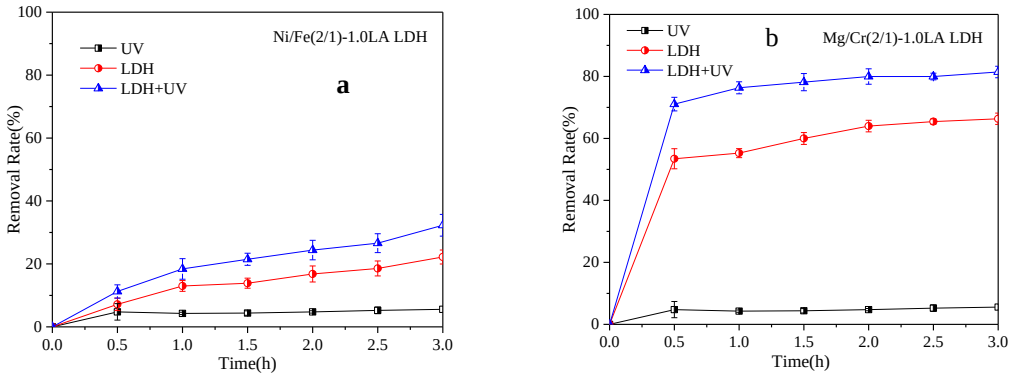


Figure 7. Photocatalytic degradation of MO over (**a**) Ni/Fe(2/1)−1.0LA LDH and (**b**) Mg/Cr(2/1)–1.0LA LDH.

Table 2. Analysis for Ni/Cr(2/1)−1.0LA LDH, Mg/Cr(2/1)−1.0LA LDH, and Ni/Fe(2/1)−1.0LA LDH.

LDH Samples	Ni^{2+} (mg/g)	Cr^{3+} (mg/g)	Mg^{2+} (mg/g)	Fe^{3+} (mg/g)	$n(M^{2+})/n(M^{3+})$	D (nm)	Band Gap (eV)
Ni/Cr(2/1)-1.0LA LDH	230.7	112.7	/	/	1.81	9.45	4.31
Ni/Fe(2/1)-1.0LA LDH	237.6	/	/	123.3	1.86	11.4	4.13
Mg/Cr(2/1)-1.0LA LDH	/	175.2	160.1	/	1.98	24.7	4.92

2.4. Mechanism of MO Degradation

The calculated photocatalytic apparent degradation rate constant, k_{app}, and the linear regression coefficients (R^2) are provided in Table 3. The Langmuir–Hinshelwood kinetic model that followed the pseudo-first-order reaction of MO photodegradation and time profiles of $\ln(C/C_0)$ for the sample is presented in Figure S3. The high values of the linear regression coefficients (R^2) indicate that the photocatalytic reaction of Ni/Cr(2/1)−0.5LA LDH was well matched with the suggested model. This means that the photocatalysis progress took place on the surface of LDH, as reported [37].

Table 3. Pseudo-first-order kinetics parameters for MO photodegradation by Ni/Cr(2/1)−0.5LA LDH.

LDH Sample	Kapp (h^{-1})	$T_{1/2}$ (h)	R^2
Ni/Cr(2/1)−0.5LA LDH	0.5471	1.26	0.99

Further, the dissolution of metals in LDH was detected, and the results are given in Table 4. With the progress in the reaction, Ni^{2+} gradually dissolved out, with 0.3% dissolution identified at the end of the photocatalytic reaction, while the dissolution of Cr^{3+} was not detected (the detection limit is 0.005 mg/L). The relatively low dissolution of Ni^{2+} indicates that the Ni/Cr(2/1)−0.5LA LDH was relatively stable in the heterogeneous phase throughout the reaction. This suggests that the photocatalytic process of Ni/Cr(2/1)−0.5LA LDH for organics degradation was mainly based on the organic-anion-intercalated LDH structure, which is performed at the surface of the catalyst. This result demonstrates that the degradation of MO was performed on the surface of Ni/Cr−LA LDH.

Table 4. Dissolution of metal of Ni/Cr(2/1)−0.5LA LDH in aqueous solution.

Metal Ions	0.5 h	1 h	1.5 h	2 h	2.5 h	3 h
Ni (%)	- *	- *	0.12	0.24	0.28	0.30
Cr (%)	- *	- *	- *	- *	- *	- *

* Under detection limit.

Our previous research found that the interlayer space of Ni/Cr−LA LDH was expanded after adsorption, and the crystallinity deteriorated [24]. This made LDH expose more metal ions and improved the utilization of the inner surface of LDH, which would enhance the photocatalysis of Ni/Cr−LA LDH.

The main active oxidation species in the photocatalytic degradation of Ni/Cr−0.5 LA LDH were verified by a quenching experiment (Figure 8). In the quenching experiment, tert-Butanol (t-BuOH), methanol, and benzoquinone (BQ) were selected as quenching agents for •OH, h^+, and $\bullet O_2^-$, respectively. As shown in Figure 8, the addition of t-BuOH and methanol had almost no influence on the degradation of MO, indicating that •OH and h^+ were not the main active oxidation species in the photocatalytic degradation of Ni/Cr-0.5LA LDH. When BQ was added to this photoreaction system, the photocatalytic degradation efficiency of MO was significantly reduced, implying that $\bullet O_2^-$ was the main active oxidation species for the degradation of MO.

According to the experimental results and previous studies, a possible mechanism of intercalated-laurate-enhanced photocatalytic activities of Ni/Cr LDHs was proposed (Figure 9). Compared to all intercalated LDHs, Ni/Cr−LA LDHs showed more activities due to several factors. One of the important factors was the interlamellar spacing. Laurate intercalation led to the increase in interlayer spacing, which provides enough interlayer space for MO entrance (Figure 1c). Moreover, laurate in the interlayer of LDH could also adsorb MO into the interlamination by partition [30]. More contact opportunities for MO and Ni/Cr LDH would benefit the degradation of MO. As shown in Figure 1b, the XRD pattern of LDH after photocatalysis displayed wider diffraction peaks compared with the unreacted sample, while the increased interlayer spacing of d_{003} reflection peaks in the sample after adsorption suggests that the interlayer spacing was expended because of the adsorption of MO molecules, which may be intercalated into the interlayer. Another

factor that enhanced the photoactivity was the crystallite size of LDHs. As shown in Table 2, the smaller crystallite size (presented as a D value that was calculated by Scherrer's formula according to the XRD pattern) of Ni/Cr(2/1)−1.0LA LDH would facilitate the rapid transfer of photo-electrons from bulk to the surface, which could effectively inhibit the recombination of photo-electrons and holes, and lead to improved photocatalytic activity. Then, the superoxide ($\bullet O_2^-$) radicals were produced by the reaction of the electron and the dissolved O_2 in the solution and further oxidized the adjacent MO molecule pre-sorbed on the intercalated LA^- in the interlayer of Ni/Cr−LA LDHs.

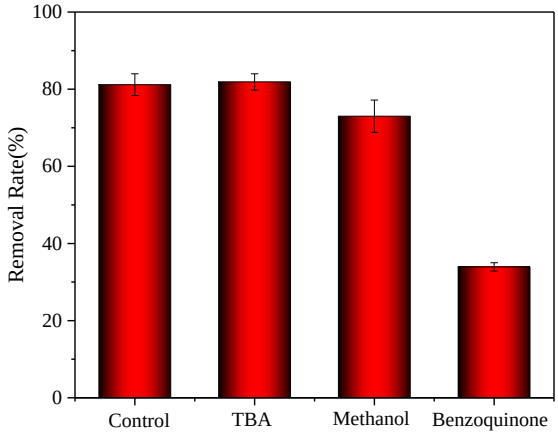


Figure 8. Photocatalytic degradation of MO over Ni/Cr(2/1)−0.5LA LDH with different free radical trapping agents.

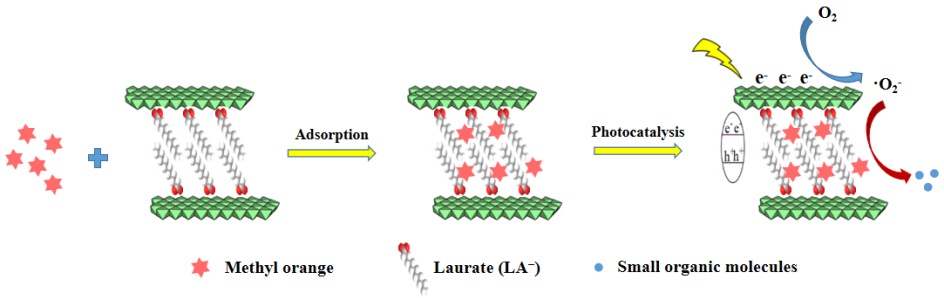


Figure 9. A possible mechanism of intercalated laurate enhanced photocatalytic activities of Ni/Cr LDHs.

3. Materials and Methods

3.1. Materials

$Cr(NO_3)_3{\cdot}9H_2O$, $Ni(NO_3)_2{\cdot}6H_2O$, $Mg(NO_3)_2{\cdot}6H_2O$, $Fe(NO_3)_3{\cdot}9H_2O$, sodium carbonate, sodium laurate, and NaOH were all purchased from Sinopharm Chemical Reagent Co., Ltd. (Shanghai, China) and used without further purification. The deionized (DI) water was used for all preparation processes under ambient conditions.

3.2. Synthesis of Ni/Cr LDHs

Organic-intercalated LDHs with different laurate concentrations (1.0 and 0.5 mol/L) were synthesized using the co-precipitation method [5] at a starting molar ratio of M^{2+}/M^{3+} = 1, 2, 3 and a final pH value of 7–8. Laurate solution was loaded into a three-necked flask (500 mL) and then placed in a water bath at 60 °C and stirred with a magnetic stirrer. A mixture (100 mL) of $Ni(NO_3)_2{\cdot}6H_2O$ (0.02 mol) and $Cr(NO_3)_3{\cdot}9H_2O$ (0.01 mol) was added dropwise to the rapidly stirred laurate solution, and the pH of the reaction was maintained at 7 by dropwise addition of aqueous NaOH (1 mol/L) until the mixed metal solution was completely added. Thereafter, the mixture was stirred for three hours, followed by aging at 65 °C for 16 h. After that, the slurry was cooled down to room

temperature and filtered; the solid residue was washed with deionized water several times and dried at 60 °C for 24 h. The dried solid was triturated with a mortar pestle, sieved through 100 meshes, and stored in sealed bags. The samples prepared were denoted as Ni/Cr−xLA LDH (Ni/Cr = 1, 2, 3), where x is the mole ratio of organic anion to Cr^{3+}.

Similarly, Ni/Fe(2/1)−1.0LA LDH and Mg/Cr(2/1)−1.0LA LDH were also prepared by using the same method mentioned above. Ni/Cr−LA LDHs with different mole ratios of Ni^{2+} and Cr^{3+} were also synthesized using the co-precipitation method except for adjusting the dosage of Ni^{2+}. Here, the mole ratio of organic anion to Cr^{3+} was 1:1. Ni/Cr−CO_3 LDH was prepared with the same method as organic LDHs, where the laurate solution was replaced by Na_2CO_3.

3.3. Photocatalytic Decolorization Process

MO was selected as the organic anion contaminant to be investigated in this study. Photocatalytic degradation of MO was performed by taking 250 mL of a 100 mg/L MO solution in a 250 mL Pyrex flask containing 0.125 g of catalyst. The solution was vigorously stirred to prevent settling of the catalyst. An 11 W low-pressure Hg lamp with a light wavelength of 254 nm was used as the light source and immersed in the solution without any filter. The temperature of the mixture was kept constant at 298 K. The photocatalytic decolorization efficiency was determined by analyzing the residual concentration of MO in the aqueous solution at different time intervals (0.5 h). Subsamples were filtered through 0.22 μm filters and measured with a U−3010 UV−vis spectrophotometer from Hitachi Limited, Co., Ltd (Tokyo, Japan) at 464 nm. A control test was also performed without the addition of the catalyst. The decolorization of MO due to adsorption was determined by carrying out a similar experiment in the dark.

The formation of intermediate active species, such as superoxide ($\bullet O_2^-$), hydroxyl radicals (•OH), and VB hole (h^+), under photoreactive conditions and their role in MO degradation, were studied indirectly by using appropriate quenches [38]. Specifically, t-butanol is a scavenger of •OH, methanol can react quickly with h^+, and benzoquinone is a scavenger of $\bullet O_2^-$. Therefore, 10 microliters of t-butanol, methanol, and benzoquinone were added to the 250 mL MO solution separately. The other detailed processes were similar to the photocatalytic experiments. All experiments were conducted in triplicates.

3.4. Characterization

In order to reveal the photocatalysis degradation mechanism of MO, the photocatalysts were separated from the solution after the photocatalytic decolorization test and were analyzed with different means.

X−ray diffraction (XRD) patterns were performed on a D/max PBX X-ray diffraction system from Rigaku Corporation, Co., Ltd (Tokyo, Japan), using Cu Kα (λ = 0.15406 nm) at 40 mA and 40 kV; a scan rate of 1°/min and a 2 Theta angle range of 1–15 degrees; and a scan rate of 8°/min and a 2 Theta angle range of 5–80 degrees.

Fourier-transform infrared spectroscopy (FTIR) spectra were recorded with a NICOLET 380 FTIR analyzer from Thermo Fisher Scientific, Co., Ltd (Waltham, MA, USA) in the range of 4000–400 cm^{-1}.

The metal concentrations in Ni/Cr LDHs were obtained by using an inductively coupled plasma atomic emission spectrometer (Prodigy ICP−AES from Leeman Co., Ltd, Hudson, NY, USA), and the samples were dissolved with dilute aqua regia prior to the analysis. The organic matter content in Ni/Cr LDHs was analyzed by using a Eurovector EA3000 automatic elemental analyzer (Eurovector, Milan, Italy).

The surface morphology of the samples was observed by a field-emission scanning electron microscope (GeminiSEM300 FE−SEM from ZEISS Co., Ltd, Oberkohen, Germany) model Nova NanoSEM 230.

The UV-visible absorption spectra of Ni/Cr LDHs were studied by using a UV-vis-NIR diffuse reflectance spectrophotometer (Shimadzu, UV-3600; 190–800 nm).

Photoluminescence of Ni/Cr LDHs was measured by using an RF−5301 fluorescence spectrometer from Shimadzu Co., Ltd (Tokyo, Japan). The excitation wavelength was set as 325 nm, and the width of the excitation and emission slit is fixed at 1 nm.

4. Conclusions

In this study, laurate-intercalated Ni/Cr LDHs were synthesized by a rapid co-precipitation method for MO photocatalytic degradation. The influence of the organic species and content on the photocatalytic performance of Ni/Cr-LA LDHs was revealed. In summary, the organic intercalated into the interlayer of LDHs was necessary in photocatalysis. Ni/Cr(2/1)-1.0LA LDH showed better photoactivity than that of Ni/Cr(2/1)-CO_3 LDH, and Ni/Cr(2/1)-0.5LA LDH exhibited the highest photoactivity. The result of reaction kinetics showed that the photocatalysis was in accordance with the pseudo-first-order kinetics, that is, the catalytic process took place on the surface of the catalyst. The organic anion expanded the interlayer space of LDH and improved the utilization of LDH's inner surface; thereby, the photocatalytic activity was enhanced by the improved adsorption of MO into the organic phase in the interlayer of Ni/Cr-LA LDH. The octahedral CrO_6 structure was found as the main photoactive site in the LDH layer. The free radical capture experiments suggest that electron-hole pairs were produced when LDH was excited by the light. The electron further reacted with O_2 in the solution to produce $\bullet O_2^-$ with high oxidation activity, and the contaminants were degraded on the surface of LDH. In future applications, Ni/Cr-LA LDH may be synthesized in situ in wastewater containing Ni^{2+} and Cr^{3+} by adding La^-. The obtained LDH could be used as a potential photocatalyst to achieve waste recycling utilization.

Supplementary Materials: The following supporting information can be downloaded at: https://www.mdpi.com/article/10.3390/catal13040698/s1, Figure S1: The XRD patterns of Ni/Cr(2/1)-CO_3 LDH; Figure S2: SEM image of (a) Ni/Cr(2/1)-1.0LA LDH and (b) Ni/Cr(2/1) LDH; Figure S3: First-order kinetics parameters for MO photodegradation by Ni/Cr(2/1)-0.5LA LDH; Table S1: Number of layers of different kinds of Ni/Cr-1.0LA LDH (Ni/Cr = 1, 2, and 3).

Author Contributions: Data curation, F.S.; formal analysis, X.Z.; funding acquisition, X.R.; investigation, F.S.; methodology, F.S.; supervision, G.Q.; validation, X.R.; visualization, Z.J.; writing—original draft, X.Z.; writing—review and editing, Z.J., Y.C., C.S., Z.Z. and X.R. All authors have read and agreed to the published version of the manuscript.

Funding: This project was supported by the National Key Research and Development Program of China (No. 2020YFC1808103), the National Nature Science Foundation of China (No. 20907029; no. 21577085).

Data Availability Statement: The research data can be acquired from the corresponding author upon reasonable request.

Conflicts of Interest: The authors declare no conflict of interest.

References

1. Xu, X.; Li, Y.; Zhang, G.; Yang, F.; He, P. NiO-$NiFe_2O_4$-rGO magnetic nanomaterials for activated peroxymonosulfate degradation of rhodamine B. *Water* **2019**, *11*, 384. [CrossRef]
2. Wu, M.J.; Wu, J.Z.; Zhang, J.; Chen, H.; Zhou, J.Z.; Qian, G.R.; Xu, Z.P.; Du, Z.; Rao, Q.L. A review on fabricating heterostructures from layered double hydroxides for enhanced photocatalytic activities. *Catal. Sci. Technol.* **2018**, *8*, 1207–1228. [CrossRef]
3. Yang, Z.; Wang, F.; Zhang, C.; Zeng, G.; Tan, X.; Yu, Z.; Zhong, Y.; Wang, H.; Cui, F. Utilization of LDH-based materials as potential adsorbents and photocatalysts for the decontamination of dyes wastewater: A review. *RSC Adv.* **2016**, *6*, 79415–79436. [CrossRef]
4. Yin, H.; Tang, Z. Ultrathin two-dimensional layered metal hydroxides: An emerging platform for advanced catalysis, energy conversion and storage. *Chem. Soc. Rev.* **2016**, *45*, 4873–4891. [CrossRef] [PubMed]
5. Jiang, Z.; Sun, F.; Frost, R.L. Adsorption characteristics of assembled and unassembled Ni/Cr layered double hydroxides towards methyl orange. *J. Colloid Interface Sci.* **2022**, *617*, 363–371. [CrossRef]
6. Tzou, Y.M.; Wang, S.L.; Hsu, L.C.; Chang, R.R.; Lin, C. Deintercalation of Li/Al LDH and its application to recover adsorbed chromate from used adsorbent. *Appl. Clay Sci.* **2007**, *37*, 107–114. [CrossRef]

7. Baig, N.; Sajid, M. Applications of layered double hydroxides based electrochemical sensors for determination of environmental pollutants: A review. *Trends Environ. Anal. Chem.* **2017**, *16*, 1–15. [CrossRef]
8. Kuthati, Y.; Kankala, R.K.; Lee, C.H. Layered double hydroxide nanoparticles for biomedical applications: Current status and recent prospects. *Appl. Clay Sci.* **2015**, *112–113*, 100–116. [CrossRef]
9. Fan, G.; Li, F.; Evans, D.G. Catalytic applications of layered double hydroxides: Recent advances and perspectives. *Chem. Soc. Rev.* **2014**, *43*, 7040–7066. [CrossRef]
10. Mohamed, F.; Abukhadra, M.R.; Shaban, M. Removal of safranin dye from water using polypyrrole nanofiber/Zn-Fe layered double hydroxide nanocomposite (Ppy NF/Zn-Fe LDH) of enhanced adsorption and photocatalytic properties. *Sci. Total Environ.* **2018**, *640–641*, 352–363. [CrossRef]
11. Shao, M.; Han, J.; Wei, M. The synthesis of hierarchical Zn-Ti layered double hydroxide for efficient visible-light photocatalysis. *Chem. Eng. J.* **2011**, *168*, 519–524. [CrossRef]
12. Hou, Y.; Feng, X. Recent Advances in Earth-Abundant Heterogeneous Electrocatalysts for Photoelectrochemical Water Splitting. *Small Methods* **2017**, *1*, 1700090. [CrossRef]
13. Mohapatra, L.; Parida, K. A review on the recent progress, challenges and perspective of layered double hydroxides as promising photocatalysts. *J. Mater. Chem. A* **2016**, *4*, 10744–10766. [CrossRef]
14. Zhang, L.; Xiong, Z.; Li, L. Uptake and degradation of Orange II by zinc aluminum layered double oxides. *J. Colloid Interface Sci.* **2016**, *469*, 224–230. [CrossRef] [PubMed]
15. Zhao, Y.; Zhao, Y.; Waterhouse, G.I.N. Layered-Double-Hydroxide Nanosheets as Efficient Visible-Light-Driven Photocatalysts for Dinitrogen Fixation. *Adv. Mater.* **2017**, *29*, 35–41. [CrossRef] [PubMed]
16. Mantilla, A.; Jácome-Acatitla, G.; Morales-Mendoza, G. Photoassisted degradation of 4-chlorophenol and p-cresol using MgAl hydrotalcites. *Ind. Eng. Chem. Res.* **2011**, *50*, 2762–2767. [CrossRef]
17. Chowdhury, P.R.; Bhattacharyya, K.G. Ni/Ti layered double hydroxide: Synthesis, characterization and application as a photocatalyst for visible light degradation of aqueous methylene blue. *Dalton Trans.* **2015**, *44*, 6809–6824. [CrossRef] [PubMed]
18. Yan, Z.; Yu, X.; Han, A. Noble-metal-free $Ni(OH)_2$-modified CdS/reduced graphene oxide nanocomposite with enhanced photocatalytic activity for hydrogen production under visible light irradiation. *J. Phys. Chem. C* **2014**, *118*, 22896–22903. [CrossRef]
19. Parida, K.; Mohapatra, L.; Baliarsingh, N. Effect of Co2+ Substitution in the Framework of Carbonate Intercalated Cu/Cr LDH on Structural, Electronic, Optical, and Photocatalytic Properties. *J. Phys. Chem. C* **2012**, *116*, 22417–22424. [CrossRef]
20. Meng, Y.; Luo, W.; Xia, X.; Ni, Z. Preparation of Salen-Metal Complexes (Metal = Co or Ni) Intercalated ZnCr-LDHs and Their Photocatalytic Degradation of Rhodamine B. *Catalysts* **2017**, *7*, 142. [CrossRef]
21. Xu, S.; Yan, H.; Wei, M. Band Structure Engineering of Transition-Metal-Based Layered Double Hydroxides toward Photocatalytic Oxygen Evolution from Water: A Theoretical- Experimental Combination Study. *J. Phys. Chem. C.* **2017**, *121*, 2683–2695. [CrossRef]
22. Liu, X.; Zhao, X.; Zhu, Y. Experimental and theoretical investigation into the elimination of organic pollutants from solution by layered double hydroxides. *Appl. Catal. B* **2013**, *140–141*, 241–248. [CrossRef]
23. Ruan, X.; Huang, S.; Chen, H. Sorption of aqueous organic contaminants onto dodecyl sulfate intercalated magnesium iron layered double hydroxide. *Appl. Clay Sci.* **2013**, *72*, 96–103. [CrossRef]
24. Ruan, X.; Chen, Y.; Chen, H. Sorption behavior of methyl orange from aqueous solution on organic matter and reduced graphene oxides modified Ni-Cr layered double hydroxides. *Chem. Eng. J.* **2016**, *297*, 295–303. [CrossRef]
25. Chaara, D.; Bruna, F.; Ulibarri, M.A. Organo/layered double hydroxide nanohybrids used to remove non ionic pesticides. *J. Hazard. Mater.* **2011**, *196*, 350–359. [CrossRef]
26. Chai, H.; Xu, X.; Lin, Y. Synthesis and UV absorption properties of 2,3-dihydroxynaphthalene-6-sulfonate anion-intercalated Zn-Al layered double hydroxides. *Polym. Degrad. Stab.* **2009**, *94*, 744–749. [CrossRef]
27. Ahmed, A.A.A.; Talib, Z.A.; Hussein, M.Z. Influence of sodium dodecyl sulfate concentration on the photocatalytic activity and dielectric properties of intercalated sodium dodecyl sulfate into Zn-Cd-Al layered double hydroxide. *Mater. Res. Bull.* **2015**, *62*, 122–131. [CrossRef]
28. Wang, B.; Zhang, X.; Liu, Y.; Li, D.; Lin, Y. Basic intensity regulation of layered double oxide for CO_2 adsorption process at medium temperature in coal gasification. *Chem. Eng. J.* **2022**, *446*, 136842. [CrossRef]
29. Smalenskaite, A.; Pavasaryte, L.; Yang, T.; Kareiva, A. Undoped and Eu3+ Doped Magnesium-Aluminium Layered Double Hydroxides: Peculiarities of Intercalation of Organic Anions and Investigation of Luminescence Properties. *Materials* **2019**, *12*, 736. [CrossRef]
30. Harada, K.; Nguyen, T.K.N.; Matsui, Y.; Fujii, K.; Grasset, F.; Ohashi, N.; Matsuda, M.; Uchikoshi, T. Observation of stacking faults and photoluminescence of laurate ion intercalated Zn/Al layered double hydroxide. *Mater. Lett.* **2018**, *213*, 323–325. [CrossRef]
31. Xia, S.; Qian, M.; Zhou, X. Theoretical and experimental investigation into the photocatalytic degradation of hexachlorobenzene by ZnCr layered double hydroxides with different anions. *J. Mol. Catal.* **2017**, *435*, 118–127. [CrossRef]
32. Zhu, Y.; Laipan, M.; Zhu, R. Enhanced photocatalytic activity of Zn/Ti-LDH via hybridizing with C60. *J. Mol. Catal.* **2017**, *427*, 54–61. [CrossRef]
33. Nakamura, R.; Okamoto, A.; Osawa, H. Design of All-Inorganic Molecular-Based Photocatalysts Sensitive to Visible Light Ti(IV)-O-Ce(III) Bimetallic Assemblies on Mesoporous Silica. *J. Am. Chem. Soc.* **2007**, *129*, 9596–9597. [CrossRef] [PubMed]
34. Baliarsingh, N.; Mohapatra, L.; Parida, K. Design and development of a visible light harvesting Ni-Zn/Cr-CO_3^{2-} LDH system for hydrogen evolution. *J. Mater. Chem. A* **2013**, *1*, 4236–4243. [CrossRef]

35. Fragoso, J.; Pastor, A.; Yustai, M.; Martin, F.; Miguel, G.; Pavlovic, I.; Sanchez, M.; Sanchez, L. Graphene quantum dots/NiTi layered double hydroxide heterojunction as a highly efficient De-NOx photocatalyst with long persistent post-illumination action. *Appl. Catal. B.* **2023**, *322*, 122115. [CrossRef]
36. Mersly, L.; Mouchtari, E.; Moujahid, E.; Forano, C.; Haddad, M.; Briche, S.; Tahiri, A.; Rafqah, S. ZnCr-LDHs with dual adsorption and photocatalysis capability for the removal of acid orange 7 dye in aqueous solution. *J. Sci.-Adv. Mater. Dev.* **2021**, *6*, 118–126. [CrossRef]
37. Ren, Z.; Xie, J.; Li, X.; Guo, L.; Zhang, Q.; Wu, J.; Li, Y.; Liu, W.; Li, P.; Fu, Y.; et al. Rational design of graphite carbon nitride-decorated zinc oxide nanoarrays on three-dimensional nickel foam for the effificient production of reactive oxygen species through stirring-promoted piezo-photocatalysis. *J. Colloid Interface Sci.* **2023**, *632*, 271–284. [CrossRef]
38. Li, D.; Long, M.; Zhao, Q. Synergetic effect of photocatalysis and peroxymonosulfate activation by $CoTiO_c$/SBA-15, $NiTiO_3$/SBA-15 and Fe_2TiO_5/SBA-15 for efficient photocatalytic removal of oxytetracycline hydrochloride. *Environ. Sci. Water Res. Technol.* **2022**, *8*, 1763–1776. [CrossRef]

Disclaimer/Publisher's Note: The statements, opinions and data contained in all publications are solely those of the individual author(s) and contributor(s) and not of MDPI and/or the editor(s). MDPI and/or the editor(s) disclaim responsibility for any injury to people or property resulting from any ideas, methods, instructions or products referred to in the content.